Journal of Electrical Engineering & Technology
https://doi.org/10.1007/s42835-022-01236-7

INVITED PAPER

# A Study on the Effect of Rotor Bars of Induction Motor for Electric Vehicle

**Hong-Rae Noh[1] · Hui-Seong Shin[1] · Cheol-Min Kim[1] · Ki-Chan Kim[1]**

Received: 5 March 2022 / Revised: 4 August 2022 / Accepted: 11 August 2022


**Abstract**
In this paper, the shape of the rotor was analyzed to reduce the torque ripple of the traction induction motor. Induction motors have a lot of problems in manufacturing if the rotor has many slots. However, if the number of rotor slots are smaller than the number of stator slots, a relatively large torque ripple occurs. So, we keep the number of existing rotor slots and insert the auxiliary bar. This changes the characteristics of the torque ripple and magnetic flux density distribution. Auxiliary bars are inserted between the rotor slots and the material is copper. The optimization methods applied in this paper to reduce torque ripple and rotor slots are experimental design, response surface method, fast Fourier transform, and total harmonic distortion. As a result, it was analyzed that the torque ripple was reduced by using auxiliary copper bars.

**Keywords** Finite element method · Total harmonic distortion · Fast Fourier transform · Induction motor · Torque ripple · Response surface method

## 1 Introduction

Induction motors have recently been applied to electric vehicles (EVs). The requirements for electric motors used in EV's drivetrain are high efficiency and wide constant power speed range. Electric machines widely used for this purpose are induction motors and interior permanent magnet synchronous motors (IPMSM). Compared to IPMSM, induction motors for EVs have the advantage of being cheaper and easier to manufacture rotors. Unlike the rotor winding type and permanent magnet type, it has a simple structure and inherent mechanical strength. These mechanical structures are suitable for harsh environments and for high-temperature and high-speed applications. The number of rotor slots is very important due to high frequency harmonics, torque ripple, and manufacturing process. For high-speed operation, the rotor of an induction motor requires many rotor slots. Therefore, it is difficult to make many rotor slots due to increased cost and increased torque ripple. Torque ripple can increase acoustic noise and mechanical vibration. It is generally undesirable in electrical machines because it can cause vibration and noise and shorten the life of the machine [1–3].

In this paper, 225 kW an induction motor of EV is designed using finite element method (FEM) for characteristic comparison analysis between 36 slots rotor of induction motor and 72 slots rotor of the proposed model[4–7]. A base model of induction motor with 36 slots rotor design can also be split into several rotor design parts, creating a rotor structure and using the auxiliary copper bar. These models deal with the parameter of rotor structure to find good characteristics [8–10]. The optimization methods applied in this paper to reduce the torque ripple of the initial model and increase the efficiency are experimental design, RSM, FFT, and THD [11–17].

## 2 Analysis Model

Figure 1 shows the proposed model of IM studied in this paper. Auxiliary bars are inserted between rotor slots to adjust low magnetic flux density and power density. The

✉ Ki-Chan Kim
kckim@hanbat.ac.kr

Hong-Rae Noh
nhrnhr1230@naver.com

Hui-Seong Shin
gmltjd9850@naver.com

Cheol-Min Kim
oo4818@naver.com

[1] Department of Electrical Engineering, Hanbat National University, Daejeon, Korea

Published online: 24 August 2022

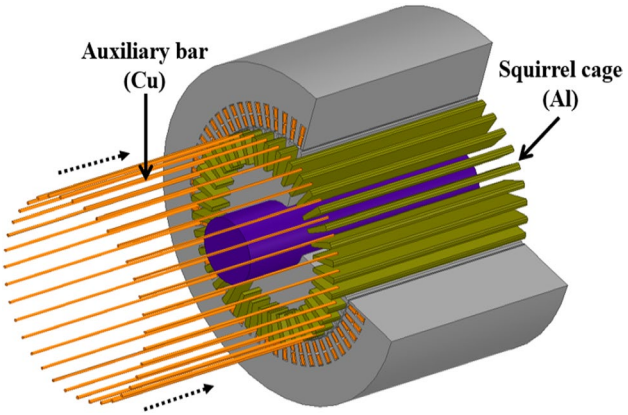


**Fig. 1.** 3D suggestion diagram of analytical model

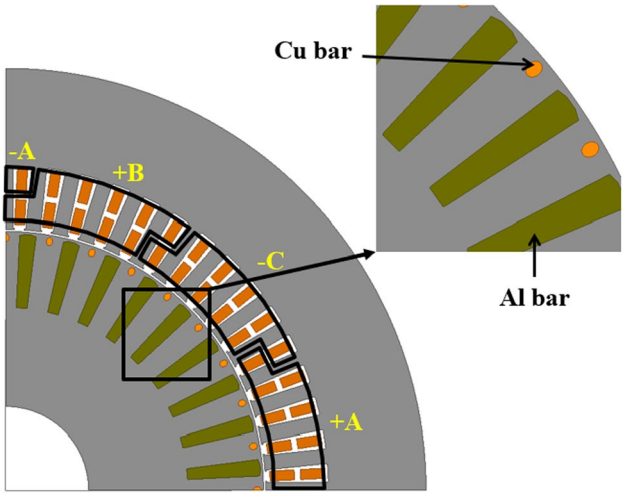


**Fig. 2.** 2D analysis model of IM

proposed model's air-gap flux density is more improved than the 36 slots rotor.

Figure 2 is a 2D quarter model of a 225 kW IM consisting of 36 aluminum bars and 36 auxiliary bars using FEM. The volume of the aluminum bar, the base model, is the same as the proposed model. A diagonal pattern appears at the connected part of the end ring. The aluminum bar and the auxiliary bar are connected by an end ring which is aluminum in Fig. 2.

Generally, the interpretation of IM is carried out using analytical methods. However, the analytical method of mathematical models makes it difficult to consider the magnetic saturation of cores. The FEM should be used for accurate analysis of voltage and frequency information for control.

The rated torque is 429.7 Nm and the limit of the rated line voltage is 220 $V_{rms}$. Detailed specifications of the model are shown in Table 1.

**Table 1** Specification of base model

| Parameters | | Specification | Unit |
|---|---|---|---|
| Rated power | | 225 | kW |
| Rated torque | | 429.7 | Nm |
| Base speed | | 5000 | rpm |
| Maximum speed | | 9000 | rpm |
| Battery voltage | | 360 | $V_{dc}$ |
| Stator | Num. of poles | 4 | Pole |
| | Outer dia. of stator | 254 | mm |
| | Num. of slots | 60 | – |
| Rotor | Outer dia. of rotor | 155.8 | mm |
| | Num. of slots | 36 | – |

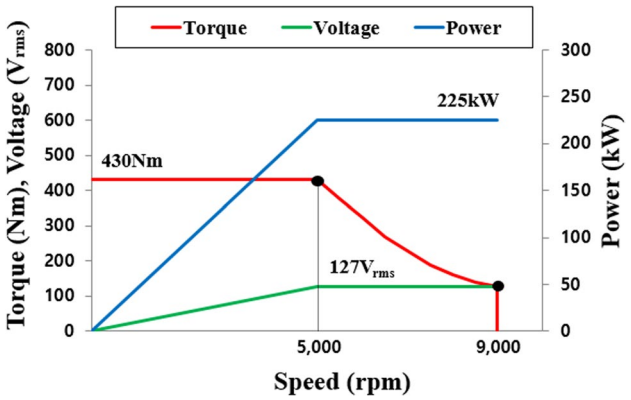


**Fig. 3** Driving performance curve of traction motor

Figure 3 shows the torque, voltage, and power of the proposed model. The rated operating point is 5000 rpm and the high-speed operating point is 9000 rpm. The output is 225 kW and the phase voltage limit is 127 $V_{rms}$.

## 3 Proposed Model

Figure 4 shows the parameters of the auxiliary bar. Considering the bridge width, the area parameter of the auxiliary bar is also changed in the same way. The sinusoidal distribution of air-gap flux density affected the decreasing torque ripple. Since the air-gap flux density's higher-order harmonics are relatively large, it is necessary to consider the copper width as well as the copper length to suppress torque pulsations in IM.

Table 2 shows 9 models according to parameters for RSM. Auxiliary bars are inserted in each model. Therefore, the characteristics of a total of 9 models were analyzed at the rated operating point of 5000 rpm. The parameters are ranged with maximum and minimum ranges considering

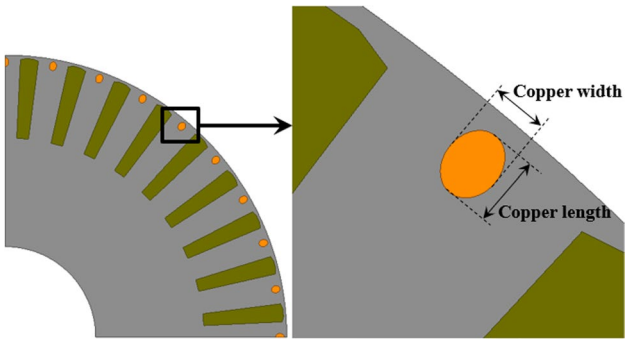


**Fig. 4** Design parameter for optimal design

**Table 2** Design variable set for RSM

| RSM model | Length | Width | Unit |
|---|---|---|---|
| 1 | 0.8 | 0.8 | mm |
| 2 | 0.8 | 0.96 | mm |
| 3 | 0.8 | 1.12 | mm |
| 4 | 1 | 1 | mm |
| 5 | 1 | 1.2 | mm |
| 6 | 1 | 1.4 | mm |
| 7 | 1.2 | 1.2 | mm |
| 8 | 1.2 | 1.44 | mm |
| 9 | 1.2 | 1.68 | mm |

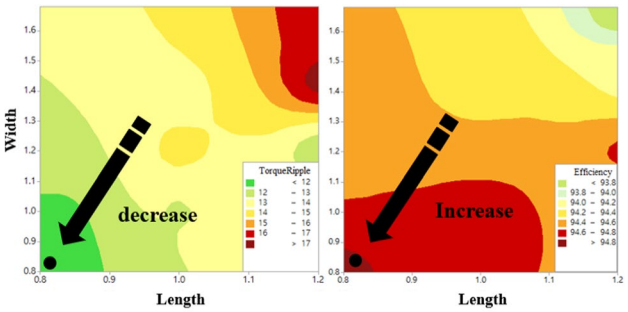


**(a)** Torque ripple **(b)** Efficiency

**Fig. 5** Analysis results on torque ripple and efficiency

manufacturing. The main characterization is focused on torque ripple and efficiency.

Figure 5 is a torque ripple and efficiency contour diagram showing the characteristics of parameters when the auxiliary bar is inserted between the rotor slots.

Figure 5a is a torque ripple contour diagram, and (b) is an efficiency contour diagram. As shown below, the closer the width and length are to the minimum, the higher the efficiency and the lower the torque ripple. Therefore, it has better characteristics than other models, so the final parameters were adopted as width 0.8 mm and length 0.8 mm.

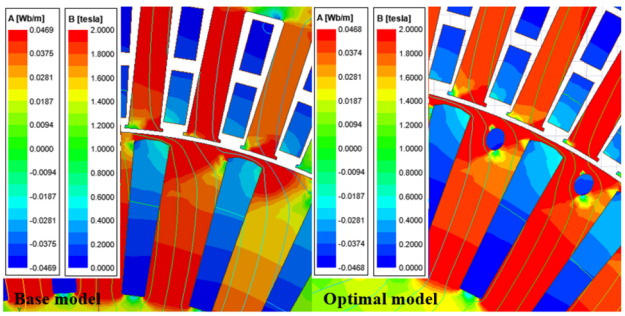


**(a)** Magnet flux density at 5,000 [rpm]

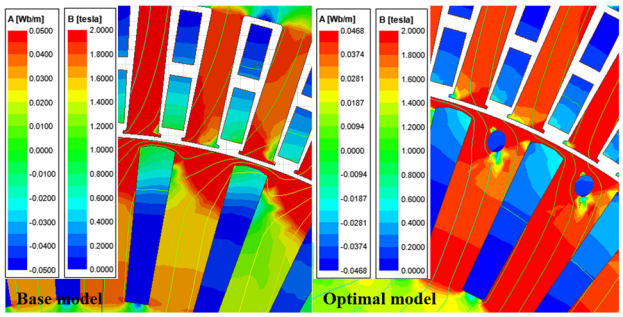


**(b)** Magnetic flux density at 9,000 [rpm]

**Fig. 6** Electromagnetic analysis results according to speed

## 4 Comparison Results

Figure 6 shows the magnetic flux densities and lines of the base and optimal models at 5000 and 9000 rpm at the same torque level. The magnetic flux density and lines of RSM model 1 are higher than that of the base model. This is because there are different magnetic flux density distributions on the rotor surface. In addition, as the rotor rotates, a sinusoidal electromotive force (EMF) occurs because the magnetic flux generated by the rotor of the optimal model is more distributed than that of the base model. Due to sinusoidal EMF, the optimal model has lower torque ripple than the base model.

Figure 7 shows the distance change of the air-gap flux density at the same point evenly distributed in the middle of the void.

The optimal model in which the auxiliary bar is inserted produces high magnetic flux density. Also, the torque of the base model is lower than that of the optimal model at the same voltage and frequency. This is because the auxiliary bar changes the magnetic flux path. The magnetic flux in the optimal model is more generated than in the base model due to the auxiliary bars between the slots. For this reason, a lower frequency can be used to produce the same torque at the same voltage.

Figure 8a compares the torque waveforms of the base and optimal model at 5000 rpm. The torque waveform at 5000 rpm shows only one electric degree cycle from 60 to 66 ms.

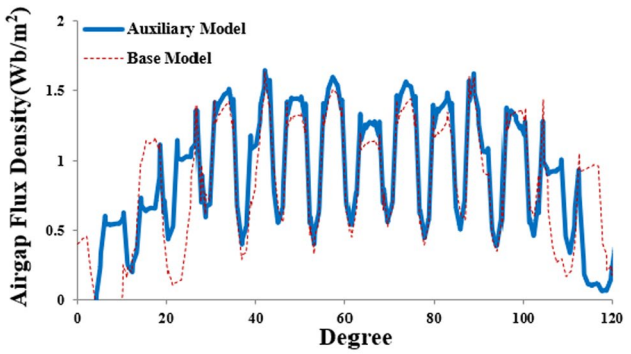


**(a)** Air-gap flux density at 5,000 [rpm]

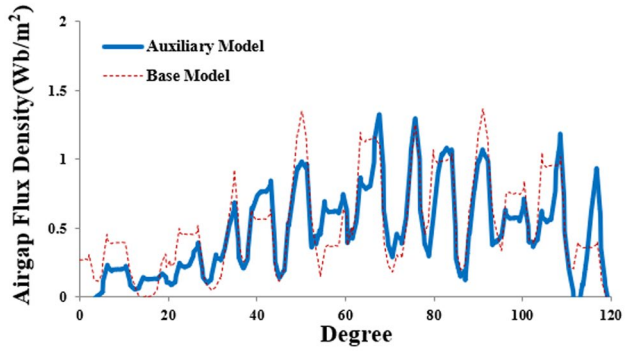


**(b)** Air-gap flux density at 9,000 [rpm]

**Fig. 7** Air-gap flux density curve analysis

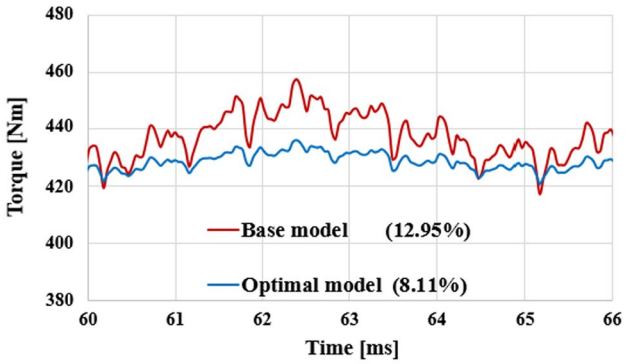


**(a)** Torque graph at 430 [Nm], 5,000 [rpm]

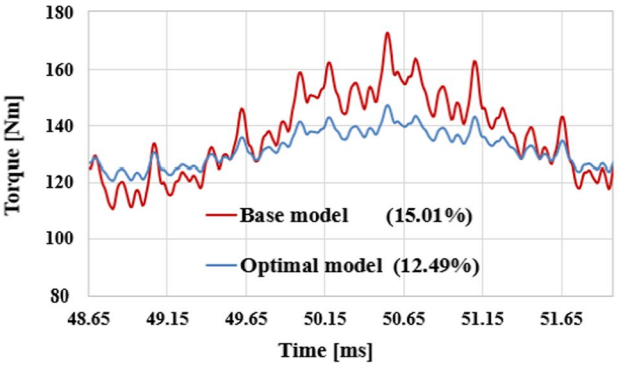


**(b)** Torque graph at 130 [Nm], 9,000 [rpm]

**Fig. 8** Torque comparison between base and optimal model

Figure 8b compares the torque waveform at 9000 rpm and shows one electric degree cycle from 48.65 to 51.98 ms. Torque ripple decreased by 4.84% at 5000 rpm and 2.52% at 9000 rpm.

As a result, the optimal model with inserted auxiliary bar has a wider range of motion than other models.

In Fig. 9, FFT analysis was performed to analyze the largest factor of torque ripple. Figure 9 shows the results of FFT analysis for torque ripple of the base and optimal models at 5000 rpm and 9000 rpm. The torque ripple is greater when the air-gap flux is not sinusoidal. This means that at 5000 rpm, the torque ripple has the greatest effect on the 3rd and 15th harmonics. For the base model, under high load conditions, the air-gap flux density generates more harmonics, resulting in more torque ripple. Figure 10 shows at 9000 rpm, 3rd harmonic and 15th harmonic are reduced by inserting the auxiliary bar.

The THD of the optimal model with auxiliary bar is 17.25%, which is lower than the base model at 5000 rpm. The optimal model is also 11.7%, which is lower than the base model at 9000 rpm.

At 5000 rpm, 9000 rpm, the slip is reduced, or the speed is increased by using auxiliary bars. As the slip decreases, the iron loss increases, but in Fig. 11, decreasing the copper loss increases the motor efficiency.

As shown in Fig. 11, at 5000 rpm, the maximum efficiency point appeared in the section where it decreased by 0.03 slip, and at 9000 rpm, it appeared in the section where it decreased by 0.04 slip. Although the speed of the rotating magnetic field did not change, the decrease in slip means that the speed of the rotor increased, and the electromotive force induced in the rotor by the auxiliary bar increased. In addition, the maximum efficiency point appears at a smaller slip, which means that the operation section is increased, and the efficiency is increased. The total content of the 3rd and 15th harmonics, which have the greatest effect on the reduction of total harmonic distortion, is expressed as the following formula.

$$\xi_D = \sqrt{\left|3^{\text{rd}}\ \text{harmonic}\right|^2 + \left|15^{\text{th}}\ \text{harmonic}\right|^2}\Big|_{Base} \tag{1}$$

$$\xi_{DO} = \sqrt{\left|3^{\text{rd}}\ \text{harmonic}\right|^2 + \left|15^{\text{th}}\ \text{harmonic}\right|^2}\Big|_{Optimal} \tag{2}$$

In (1), (2) where the 3rd harmonic and 15th harmonic are the values expressed as the average of the values from 0 to 360 rad by taking the absolute value. To find the THD change rate is multiplied by applying the auxiliary bar:

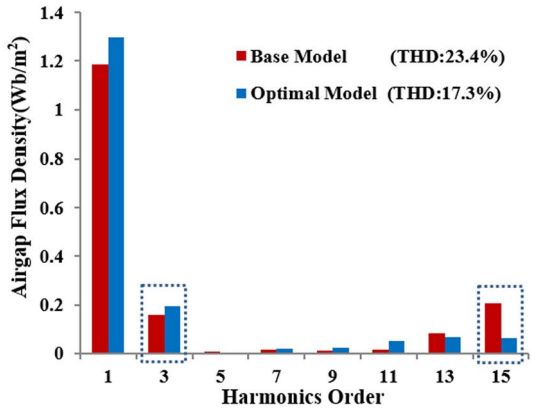


**(a)** Total Harmonic distortion at 430 [Nm], 5,000 [rpm]

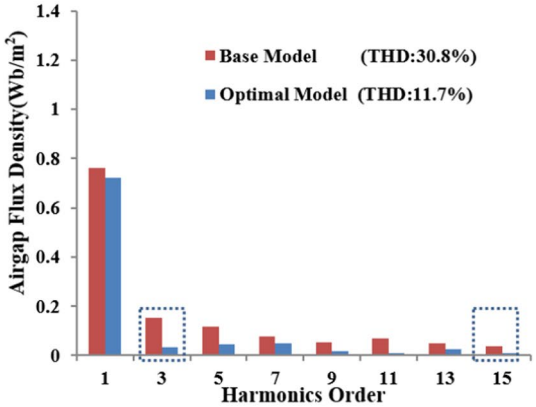


**(b)** Total harmonic distortion at 130 [Nm], 9,000 [rpm]

**Fig. 9** THD analysis of air-gap density by FFT

$$K_{\xi}=\frac{\xi_{DO}}{\xi_{D}}=\frac{0.02359}{0.10171}=0.232 \tag{3}$$

where the $K_{\xi}$ means the ratio of total content of harmonic distortion. Multiplying $K_{\xi}$ by the amount of slip reduction gives the rate of change in speed at the point of slip reduction:

$$\Delta_{speed}=K_{\xi}\times\text{Slip Difference} \tag{4}$$

Then, $\Delta_{base\_speed}$ goes to $6.96\times10^{-3}$ and $\Delta_{max\_speed}$ goes to $9.28\times10^{-3}$. Now that we have found the two points of the rate of change in speed due to change in slip reduction rate, we can draw a straight line to convert it to a function:

$$y=(5.8\times10^{-4})x+4.06 \tag{5}$$

By substituting an arbitrary rotor speed into x, it is converted to the rotor speed in the optimal model. Using (5), you can easily find the driving section of the optimal model, and the time required to find all the driving sections can be further saved by interpolation.

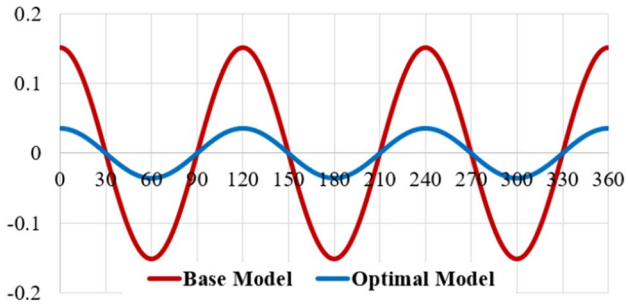


**(a)** 3rd harmonic comparison graph at 9,000 [rpm]

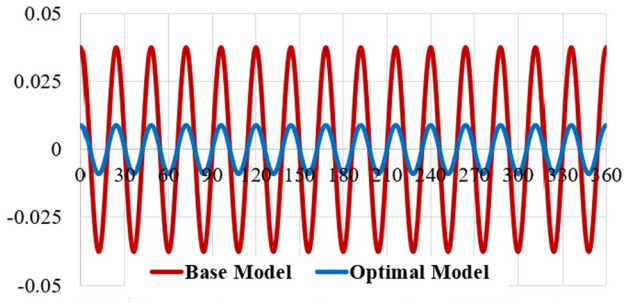


**(b)** 15th harmonic comparison graph at 9,000 [rpm]

**Fig. 10** Harmonics comparison between base and optimal model at 9000 rpm

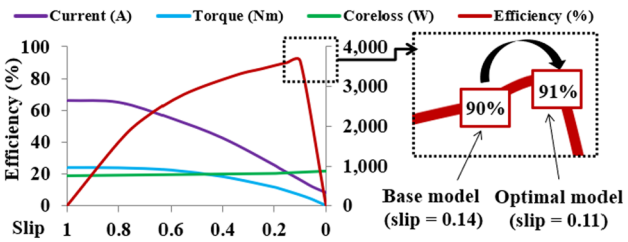


**(a)** Slip curve of constant torque region at 430 [Nm]

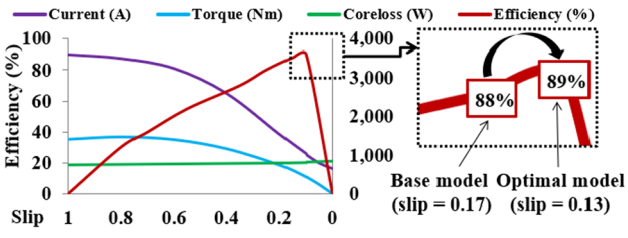


**(b)** Slip curve of constant torque region at 130 [Nm], 9,000 [rpm]

**Fig. 11** Comparison of results between base and optimal model on the slip characteristics

## 5 Conclusion

Based on these results, the proposed smooth torque and high-efficiency method is to generate sufficient magnetic flux in the rotor using an auxiliary bar. This is caused by

the change in magnetic flux density in space relative to the rotor surface. This is because the auxiliary bar changes the magnetic flux path. The magnetic flux in the optimal model is more generated than in the base model due to the auxiliary bars between the slots. For this reason, a lower frequency can be used to produce the same torque at the same voltage. As a result, the operating range of the optimal model with inserted auxiliary bar is wider than that of the base model. Total Harmonic distortion and air-gap flux density distributions were also demonstrated. Therefore, inserting the auxiliary bar between the rotor slots to solve the low magnetic flux density and power density effectively reduces the output torque ripple.

Finally, a formula that can similarly derive a new operation section of the optimal model by investing a short analysis time was proposed. The proposed formula will have different constant values for each model, but the process of deriving the $\xi_D$, $K_\xi$, and $\Delta_{speed}$ are universal. Reducing analysis time is directly related to increasing work efficiency from the motor designer's point of view, so it can be very effective. It will be possible to quickly verify the efficacy of the improved model in various types of motors as well as IM, and it is thought that it will contribute to the development of the motor industry.

**Acknowledgements** This work was supported by the Korea Institute of Energy Technology Evaluation and Planning (KETEP) and the Ministry of Trade, Industry & Energy (MOTIE) of the Republic of Korea (No.20204030200080).

**Declaration**

**Conflict of interest** On behalf of all authors, the corresponding author states that there is no conflict of interest.

## References

1. Victor VF, Quintaes FO, Lopes JS, Junior LDS, Lock AS, Salazar A (2012) O, Analysis and study of a bearingless AC motor type divided winding, based on a conventional squirrel cage induction motor. IEEE Trans Magn 48(11):571–3574
2. Nerg J, Pyrhönen J, Partanen J (2004) Finite element modeling of the magnetizing inductance of an induction motor as a function of torque. IEEE Trans Magn 40(4):2047–2049
3. Zhang P, Yi Du, Habetler TG, Bin Lu (May 2011) Magnetic effects of DC signal injection on induction motors for thermal evaluation of stator windings. IEEE Trans Ind Electron 45(5):1479–1489
4. Lee G, Min S, Hong J-P (May 2013) Optimal shape design of rotor slot in squirrel-cage induction motor considering torque characteristics. IEEE Trans Magn 49(5):2197–2200
5. Faiz J, Ebrahimi BM, Akin B, Toliyat HA (2007) Finite-element transient analysis of induction motors under mixed eccentricity fault. IEEE Trans Magn 44(1):66–74
6. Zhang D, Park CS, Koh CS (2012) A new optimal design method of rotor slot of three-phase squirrel cage induction motor for NEMA class D speed-torque characteristic using multi-objective optimization algorithm. IEEE Trans Magn 48(2):879–882
7. Vamvakari A, Kandianis A, Kladas A, Manias S (1999) High fidelity equivalent circuit representation of induction motor determined by finite elements for electribat vehicle drive applications. IEEE Trans Magn 35(3):1857–1860
8. Boglietti A, Bojoi RI, Cavagnino A, Guglielmi P, Miotto A (2012) Analysis and modeling of rotor slot enclosure effects in high-speed induction motors. IEEE Trans Ind Appl 48(4):1279–1287
9. Faiz J, Ebrahimi B-M (2008) A new pattern for detecting broken rotor bars in induction motors during start-up. IEEE Trans Magn 44(12):4673–4683
10. Climente-Alarcon V, Antonino-Daviu JA, Strangas EG, Riera-Guasp M (2014) Rotor-bar breakage mechanism and prognosis in an induction motor. IEEE Trans Ind Electron 62(3):1814–1825
11. Mohammed OA, Abed NY, Ganu S (2006) Modeling and characterization of induction motor internal faults using finite-element and discrete wavelet transforms. IEEE Trans Magn 42(10):3434–3436
12. Kim D-J, Hong D-K, Choi J-H, Chun Y-D, Woo B-C, Koo D-H (2013) An analytical approach for a high speed and high efficiency induction motor considering magnetic and mechanical problems. IEEE Trans Magn 49(5):2319–2322
13. Jeon WJ, Katoh S, Iwamoto T, Kamiya Y, Onuki T (1999) Propulsive characteristics of a novel linear hybrid motor with both induction and synchronous operations. IEEE Trans Magn 35(5):4025–4027
14. Ergene LT, Salon SJ (2005) Determining the equivalent circuit parameters of canned solid-rotor induction motors. IEEE Trans Magn 41(7):2281–2286
15. Noh HR, Shin HS, Kim CM, Kim KC (2021) A study on the effect of rotor bars of induction motor for electric vehicle. In: 2021 24th international conference on electrical machines and systems (ICEMS), pp 1415–1418. IEEE
16. Kim JH, Jung YG (2021) Spreading power spectrum of an induction motor drive system by chaotic pulse width modulation method. J Electr Eng Technol 16(5):2685–2694
17. Chandrasekaran S, Durairaj S, Padmavathi S (2021) A performance improvement of the fuzzy controller-based multi-level inverter-fed three-phase induction motor with enhanced time and speed of response. J Electr Eng Technol 16(2):1131–1141



**Hong-Rae Noh** He received B.S degree in el ectrical engineering from Hanbat National university. His research interests are design and analysis of electrical machinery.

**Hui-Seong Shin** He receive d B.S degree in el ectrical engineering from Hanbat National university. His research interests are design and analysis of electrical machinery.

**Cheol-Min Kim** He received B.S degree in el ectrical engineering from Hanbat National university. His research interests are design and analysis of electrical machinery.

**Ki-Chan Kim** He received B.S , M.S, and Ph.D degree s in el ectrical engineering from Han y ang university. He worked at the Electro Mechanical Research Ins titute of Hyundai H eavy Industries Co., Ltd. as a Senior Researcher Now he is a Professor in Electrical E ngineering at Hanbat National University His research interests are design and analysis of el ectrical machinery.